# 6

# Conclusions and future work

*"From out there on the Moon, international politics look so petty. You want to grab a politician by the scruff of the neck and drag him a quarter of a million miles out and say, 'Look at that, you son of a bitch'."*

– Edgar Mitchel, Apollo 14 astronaut, People magazine, 8 April 1974

## 6.1 Thesis conclusions

This thesis has focussed on lifting the veil on the shape of our Galaxy, a problem that has plagued observers and theorists alike for decades. The method to do so was to utilise numerical SPH simulations to model the ISM evolution in a Milky Way-like disc. Many different Milky Way models were employed, investigating a wide variety of morphologies of the bar and spiral arms. Using these simulations, synthetic observations (primarily of CO emission) were then created using a radiative transfer code which could be directly compared to observational data. By finding models that provide a good representation of the emission features of our Galaxy it was inferred whether the morphology of the input Galaxy model was a good representation of the Milky Way's morphology. Whilst other authors have produced individual synthetic maps from simulations, here we extend this idea to using multiple simulations to carry out a systematic study of the available parameter space and use a full radiative transfer treatment to replicate observations.

In Chapters 1 and 2 we set the scene of the problem at hand and present the primary numerical tool used throughout this work; SPH. This includes the specialised physics and chemistry incorporated that allows for ISM cooling and molecular gas formation, which is key for creation of the synthetic observations.

In Chapter 3 results are presented where the Galaxy is assumed to be grand design in nature,

i.e. that the morphology is fixed and unchanging in nature with distinct arm and bar features. The gas in a Galactic disc is subjected to a variety of different analytic potentials designed to represent the stellar gravitational field of the main morphological components. Separate simulations using arms or bars are first performed, investigating the effect of pattern speeds, bar orientation, arm number and arm pitch angle on structures seen in longitude-velocity space. Best-fitting values for the bar favour pattern speeds of $50 - 60 \text{km s}^{-1} \text{kpc}^{-1}$ and orientations of $\approx 45°$, while the best-fitting values for the arms are a pattern speed of $20 \text{km s}^{-1} \text{kpc}^{-1}$ and a pitch angle from $10° - 15°$. Some of the parameters showed clear best fits, such as arm pattern speed, while others were harder to constrain, such as the pitch angle. Bars and arms on their own could not provide a good match for observations, with the position of resonances limiting the radial extent structures could be sustained in the gas. Specifically, a fast bar was needed to produce features in the inner disc, while arms of a much slower pattern speed were needed to observe arms beyond the Solar radius. The observer's position and velocity were also variables in the modelling as they could heavily impact the position of emission features. While not the subject of our investigation, best-fitting models showed a good agreement with literature values.

Synthetic observations in Chapter 3 were calculated in a very simple manner. In Chapter 4 this is greatly improved by use of a radiative transfer code which explicitly calculated the emissivity and opacity throughout the model galaxies. Synthetic observations showed that molecular emission features were highly sensitive to the surface density of the gas, which directly determines its column density and optical thickness. Emission from arms and bars was visible in our fiducial gas disc, though the peak brightness temperatures were somewhat greater than those observed. H I emission on the other hand did not trace the morphology well. This is believed to be caused by the gas settling into a very narrow range of latitudes, which causes very high atomic gas column densities, a problem induced by the simplistic nature of the potentials. This was not an issue with CO, as the molecular gas density is so much lower than that of the H I. Simulations were then performed with the best-fitting arms and bars from Chapter 3. Many of the emission features from the Milky Way were reproducible, such as various individual spiral arms. There was however no model that could fit all features simultaneously. The primary difficulty was in reproducing the Carina arm in the fourth quadrant and the inner molecular ridge of material with the correct orientation in *l-v* space inside $|l| < 50°$. In order to match Carina using fixed logarithmic spirals the arm must pass in between the observer and the Galactic centre, creating a great swath of emission and local velocities ($v_{los} \approx 0 \text{km s}^{-1}$), which is not seen in observations. Either the molecular gas in this arm must be greatly reduced, by this arm perhaps being weaker in general to others, or the shape must stray from logarithmic in the Solar vicinity. The arm number, perhaps the key parameter in mapping the Galaxy, was not clearly constrained. Two armed models provided a better fit numerically, but could not fit all observed features simultaneously. Conversely four armed models could reproduce all features, but inadvertently produced spurious emission where it was not required, worsening the quality of the fit. A such we conclude a four armed barred model is a good representation of our Galaxy, but a key ingredient is needed to remove or amend some of the spurious emission features.

In Chapter 5 a different approach is taken where the analytic potentials representing the

stellar component are replaced with a system of *N*-body "star" particles, whose evolution determines the gravitational forces experienced by the gas. The resulting arm features are transient and vary greatly in shape, displaying multiple branches, inter-arm features, and kinks. The number of arms created is strongly correlated to the disc to halo mass ratio, with arm numbers ranging from two to five and in some cases producing effectively a flocculent disc. Pitch angles tend to be rather wide compared to those found using analytic potentials, with values around $20°$. These arms tend to have a pattern speed that decreases with radius, implying they are material in nature rather than standing density waves. While some bar features are also created, these are either a poor match for the inner velocity structure or do not create sufficient emission in the outer disc. The CO emission maps for our best-fitting calculations appear a much better match to the observed map than the analytic potentials, with a select few maps reproducing many of the arm structures. These best fitting models favour a four-armed structure, though interestingly a highly flocculent disc with no clear dominant spiral mode can also provide a reasonable match. The main detriment of these models is the over-abundance of emission in the Galactic centre. This may require an inner bar, absent in most of these models but present in the models using analytic potentials, to sweep up this excess molecular material in the $|l| < 20°$ region. The H I emission also provides a closer match to observations that than of the fixed potentials, due to the live-disc being greater dispersed around the Galactic plane.

In the Introduction we proposed 5 key questions we sought the answers to in this work. These questions and direct answers are as follows.

- Can we create synthetic molecular emission maps of our own Galaxy sufficient for the purpose of constraining morphology? The longitude velocity emission maps indeed proved very capable of highlighting what could be deemed a good and a poor spiral model of the Galaxy. The addition of a radiative treatment over previous studies helped to highlight the dangers of simply matching up arm features as material very near the observer can produce extremely bright emission features not seen in observations.

- Can a grand design spiral perturbation sufficiently reproduce the observed features in *l-v* space? The barred and armed models made using fixed potentials failed to provide a full match to observed features. While individual arm structures could be reproduced, the symmetric grand-design models proved incapable of matching all structures simultaneously.

- Is a 2-armed structure sufficient to reproduce all the features, or is a 4-armed model needed? A four armed pattern is required, both seen in the fixed potentials and live disc simulations. There is simply not enough structure in the gas to match the *l-v* data with two arms.

- Does a 2-armed stellar distribution produce a 4-armed gas morphology sufficient to match *l-v* features? We found that a 2-armed stellar spiral can produce 4-armed gas features, but that these are too tightly wound to match the observations. Interesting the live disc simulations produced strong $m = 2$ modes in the inner disc and strong $m = 4$ modes in the outer disc, which could be the best way to reconcile the 2 and 4-armed paradigms inferred by observations.

- Can instead a transient spiral structure better fit the observations? The material and recurrent spiral structure of the live disc simulations produced much better matches to the observa-

tional data. The more irregular arm structure coupled with more discontinuous emission along individual arms allowed for more realistic *l-v* maps, and allowed for different arm numbers to dominate different Galactic radii.

The synthetic observations in this thesis show that a four-armed morphology is needed to reproduce the observed gas emission features. The theory that a two-armed stellar morphology can drive a four-armed structure in the gas is only supported by a small amount of models with fixed potentials, and none of the calculations with a live disc. Fixed analytic potentials tend to be a poorer representation of the disc, with a live stellar distribution creating a better range of features that can match the observed arm emission implying the arms of the Milky Way may not be in a steady state driven by spiral density waves. A bar feature does seem required however in the inner disc. The inclusion of a bar in the analytic models gave a better match to inner features than the arm only models created using a live disc, which display an over-abundance of emission towards the Galactic centre. As such, modelling the Galaxy a live-stellar disc and transient arms with the inclusion of a small, rapidly rotating inner bar, would provide the best reproduction of our Galaxy.

## 6.2 Future work

The work outlined in this thesis has some clear and obvious avenues for extension. In following subsections we discuss directions we have already begun working in to either further understand the morphology of the Milky Way, or constrain some other Galactic scale features.

### 6.2.1 Perturbing bodies driving spiral structure

A mechanism of spiral structure generation that we have not investigated thus far in detail is that caused by passage of some massive perturbing body. The tidal forces on a galactic disc are believed to be very effective at seeding spiral arms, bridges and tails (Toomre & Toomre 1972; Dobbs et al. 2010). There are many examples in the literature of the effect of a perturbing mass, be it point mass or a many-body system, on a Milky Way-like disc (Toomre & Toomre 1972; Donner et al. 1991; Barnes & Hernquist 1996; Oh et al. 2008; Dobbs et al. 2010; Purcell et al. 2011; Struck et al. 2011). However, as far as we are aware there has been no in-depth study on wether these tidal effects could produce morphologies that are a good representation of our own Galaxy.

By using an *N*-body and SPH prescription, similar to Chapter 5 it is possible to simulate such a perturbing scenario. This was done so by Dobbs et al. (2010), who used a point mass perturber to simulate the interaction between a galactic disc and the creation of spiral structure that showed a striking resemblance to M51. We have already performed numerous test calculations on the effects of a point mass perturber on the discs presented in Chapter 5, an example of which is shown in Figure 6.1. Here a point mass perturbing particle with approximately a third of the mass of the stellar disc approaches the disc on a hyperbolic orbit and induces a two armed spiral feature in the disc. This spiral structure persists for about three rotations of the disc, in which time the perturber has continued on it's orbital path. This interaction also seems to have bolstered the inner bar, it appearing much longer and than in the initial time-stamp. An advantage of this
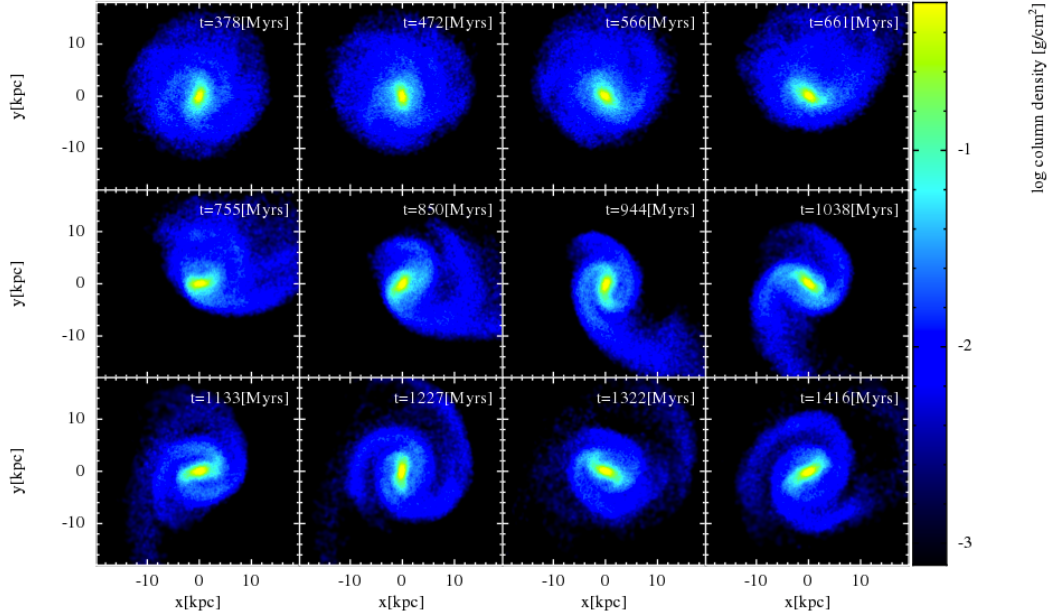
Figure 6.1: Effect of point-mass perturber on a disc galaxy composed of 1 million star particles that have formed a weak barred structure. The perturber is initially located at the top of the first panel, and moves on a hyperbolic orbit clockwise (off-panel). Its passage induces arms in the stars, which persist for three full rotations after periastron passage.

method is that it is an easy way of reproducing $m = 2$ features in the disc, which was difficult to do in the isolated galaxy case in Chapter 5. The next step is to include gas particles with active chemistry, and then construct synthetic CO emission maps to assess the validity of the models. Preliminary tests show that the velocity structure is quite different from the isolated case, with the tides caused by the perturber inducing large scale velocity structures in the disc. It may therefore be prudent to allow the disc to settle somewhat after the passage of the perturber, though this will also result in a weakening of spiral features. Extension of this method would involve replacing the point-mass perturber by an *N*-body companion, though the increase in computational cost would be considerable.

### 6.2.2 The effects of stellar feedback and self-gravity on global *l-v* features

In terms of the physics incorporated into the models in this thesis, we have taken a practically simple approach. The forces experienced by the gas are reduced to the stellar gravitational field and hydrodynamical forces, with additional ISM heating and cooling mechanisms. The main omission is the gravitational effect of the gas upon itself, which we have assumed to be negligible compared to that of the stellar system. The addition of self-gravity results in creation of clumps in the gas, and acts to create inhomogenities in the global gas flow (Dobbs 2008). To maintain a calculation involving self-gravity in the gas it is prudent to include some method of breaking up these dense clumps. To this end stellar feedback can be employed to insert energy into the ISM. This approach has been employed by numerous galactic-scale studies in the past, both in grid-based and SPH
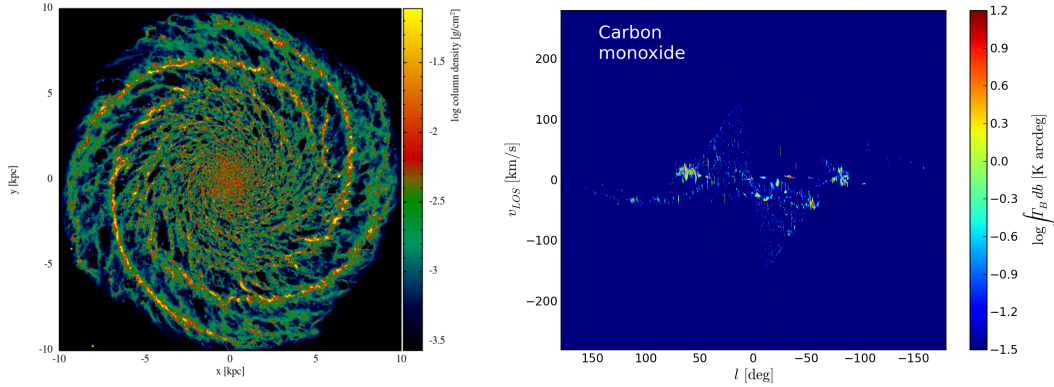
Figure 6.2: The effect of supernovae feedback and self-gravity on the evolution of the ISM disc with a 4-armed spiral potential and resulting CO emission features. The left panel shows the top-down surface density after 250Myrs of evolution and the right panel the CO emission map created using torus with the observer placed at $y = 7$kpc in the top-down view. SPH calculation performed by C. Dobbs using sphng with 8 million particles and is described in Dobbs et al. (2011).

codes; Wada et al. (2000); Scannapieco et al. (2006); Tasker & Bryan (2006); Dobbs et al. (2011); Kawata et al. (2014). Stellar feedback comes in variety of forms, be it radiation pressure, stellar winds or supernova feedback. In galactic-scale calculations this is usually solely represented by the strongest contribution; that of supernovae. These feedback events occur when the gas becomes sufficiently dense, i.e. forming a GMC. The activation of such a feedback event in the code is a costly one, and requires neighbour lists to be re-called in order to ascertain where the energy of the supernova must be deposited. Coupled with the inclusion of self-gravity, these calculations can be extremely more computationally expensive than those presented in this thesis.

The inclusion feedback can act to greatly change the global morphology of galactic simulations. As such the effect on the synthetic observations, such as those presented in this thesis, could be great. The effect of such physics has already been investigated to a degree by Duarte-Cabral et al. (in preperation) and Acreman et al. (2012), where the emission structures from fixed analytic potentials are greatly disrupted and provide a much better resemblance to observations. These studies, however, were focused solely on the second quadrant using some assumed spiral model. As an extension to the work of this thesis we intend on taking our best fit models and including the effects of self-gravity and feedback in hopes of producing an even match to observations. The code sphng (utilised in Chapter 5) has already been adapted by C. Dobbs to include supernova feedback (Dobbs et al. 2011), so utilising it with the models in Chapters 3 and 5 would be relatively straight forward. It has also been used with a live-stellar system (Dobbs et al. 2012).

As a simple test of this approach, we have taken a calculation from Dobbs et al. (2011) that includes self-gravity, feedback and four-armed potential and created a synthetic plane survey of CO emission, shown in Figure 6.2. The top-down map of the gas is shown in the left, and the torus CO *l-v* map in the right. Emission features are greatly dispersed compared to those in Chapters 4 and 5 and arm features can be seen away from the local velocity plane (note the Perseus and Carina arm analogues). The surface density of the gas is somewhat lower than our
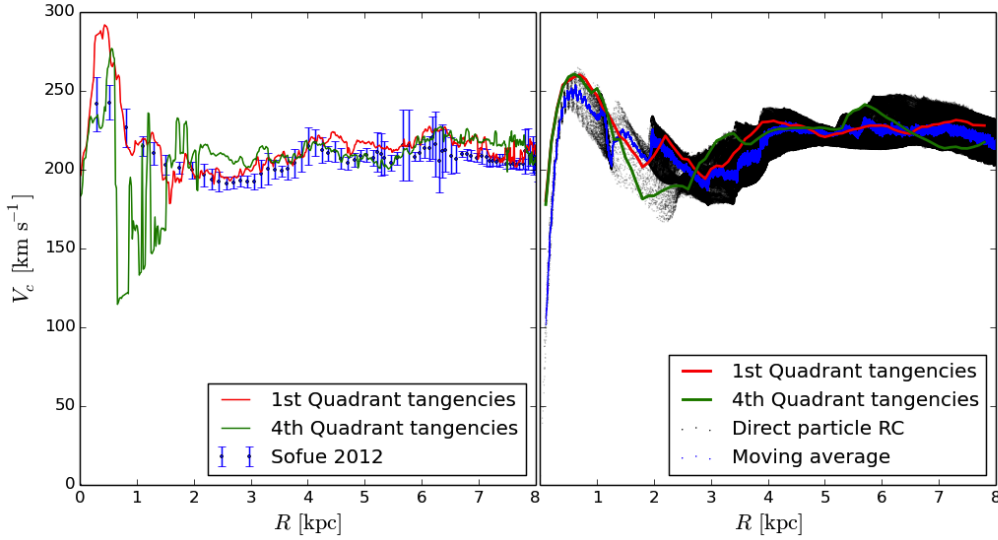
Figure 6.3: Different rotation curves from observational data of the Milky Way (left) and a barred-spiral simulation (right). In the left panel we show the rotation curve data from Sofue (2012) and rotation curves calculated from the terminal velocities of the CO *l-v* map of Dame et al. (2001) in using longitudes $0° < l < 180°$ and $180° < l < 360°$. In the right panel are similar rotation curves for the SPH calculation. The green and red lines are from 4th and 1st quadrant tangencies respectively. Black points are the circular velocities of individual SPH particles, and the blue points are these moving averages of the individual values.

calculations, which results in reduced emission overall (see Fig. 4.3). Note also the lack of any clear resonance features caused by the arms in the top down plot, which appeared clearly visible in our calculations.

An obvious question is why we did not include these effects in the first place. The answer is that self-gravity and feedback greatly increase computational time. With a vast parameter space to explore and a moderately high resolution required to produce CO emission, this would simply not have been computationally feasible.

### 6.2.3 Further tests of Galactic structure

Longitude-velocity emission maps are complex structures with which to fit our models to. The data product is effectively a 4-dimensional object, and as such the fitting procedure is quite complicated. As such it is prudent to use other observations of our Galaxy with which to constrain our models. This could involve a study specifically focussed on reproducing the *l-v* features of H I in the full Galactic plane and using a live-stellar system or feedback which would drive material away form $b = 0°$ and avoiding the problems in Section 4.4. The models already created for this thesis could also be re-used to create further synthetic observations. Arm tangency maps such as those of Drimmel (2000) or Benjamin et al. (2005) could be easily created for both static and live stellar systems. Doing so for the calculations in Chapter 5 could be compared to the studies that find significant differences in the tangencies observed in the stars and the gas (Drimmel 2000; Steiman-
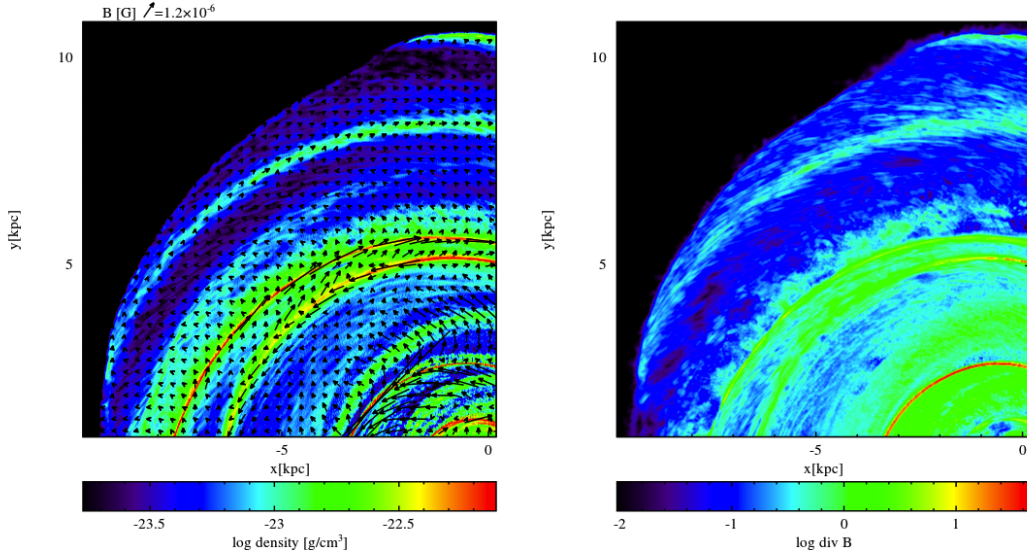
Figure 6.4: Simulation of ISM gas in a 2-armed spiral galaxy with an active magnetic field. An initial toroidal field with a strength of $B_\circ = 10^{-7}$G can be seen to be enhanced and flip directions in the left panel, where arrows indicate the direction and strength of field. In the right panel the divergence of the magnetic field is shown in the same region ($\vec{\nabla} \cdot \vec{B}$). This computation was performed using PHANTOM and 8 million SPH particles.

Cameron et al. 2010).

A simple additional comparison to make with observations is to compare the various rotation curves that can be computed from our models to those measured for our Galaxy. In Figure 6.3 we show various rotation curves for our Galaxy (left) and from a barred-spiral calculation (right). Rotation curves can be calculated directly from the terminal velocities of $l$-$v$ maps, with various dips and bumps highlighting morphological features. By simply comparing the different rotation curves, such as for example those created from the fourth quadrant tangencies from models and observations, we can infer additional information regarding Galactic morphology.

### 6.2.4   Galactic magnetic field reversal

A feature of our Galaxy that we have so far over-looked is the topology of the galactic-scale magnetic field. The existence of some field has been known for some time due to the observation of rotation measures (pulsar observations), which require some finite magnetic field. The magnetic field in disc galaxies is believed to originate either from some dynamo action on small scale turbulent field lines, or due to some primordial magnetic field. Regardless of its origin, magnetic fields have been observed in external disc galaxies with field strengths of the order of $\mu$G (Beck et al. 1996).

The topology of the magnetic field of the Milky Way is as shrouded in doubt as the arm morphology. Studies seem to present a divided opinion on whether the direction of the magnetic field lines reverse at every spiral arm passage (Sofue & Fujimoto 1983; Han et al. 2006), experience just a single reversal at Sagittarius arm (Brown 2010) or reverse in a series of Galactocentric rings (Vallée 2011). Numerical simulations on the subject have shown that an initial small scale

field can be greatly magnified and ordered by the differential rotation in the disc (Kotarba et al. 2009; Pakmor & Springel 2013). Other work has shown that the field can be disordered from the global symmetry by pockets of cold ISM gas (Dobbs & Price 2008).

An application of the best fitting spiral models presented in this thesis is to introduce a Galactic-scale magnetic field and study the effect of the field on the disc evolution. A specific goal would be to assess the plausibility of the reversal of magnetic field lines in the passage of spiral arms. Is a reversal reproducible in the Best-fitting Galactic models? If so, how is this dependant on arm number and pattern speed?

Many techniques already exist for including magnetic fields in SPH (see Price 2012a for a review). We have performed numerous preliminary simulations in collaboration with D. Price and C. Dobbs involving an active magnetic field in disc galaxies similar to those in shown in Chapter 3. In Figure 6.4 we shown one such calculation of ISM gas in a two-armed spiral galaxy. In the left panel is the density render of a single quadrant with magnetic field vectors overplotted. In the right panel the divergence of the magnetic field is shown for the same region. The calculation is performed using PHANTOM with 8 million SPH particles and an isothermal equation of state ($T = 100$K). An initial toroidal magnetic field is applied with a strength of $B_\circ = 10^{-7}$G. Somewhat promisingly, the magnetic field can clearly be seen to change orientations in the passage through the spiral arms. In the two-armed brach region the field seems to swap from being directed towards then opposite to the disc rotation. The right panel illustrates a problem with these calculations. The divergence of the field is clearly non-zero throughout the disc, with values in the inner arms especially reaching considerable magnitudes. While methods such as additional divergence cleaning can improve matters, these calculations usually crash in an explosion of $\vec{\nabla} \cdot \vec{B}$. A possible work-around is to allow the disc to settle considerably before the activation of a magnetic field, and preliminary tests show this allows for simulation of the magnetic field for many Gyr without incident.